Auto-Physics-Encoder: Using Physics-Informed Latent Layer Two-Way Physics Flow for Monitoring Systems with Unobservability

Priyabrata Sundaray SUNDARAY@ASU.EDU
Arizona State University, Tempe, AZ, USA

Yang Weng YANG.WENG@ASU.EDU
Arizona State University, Tempe, AZ, USA

Editors: Emtiyaz Khan and Mehmet Gönen

Abstract

With the Internet of Everything (IoE) nowadays, monitoring edge systems is essential for coordinating everything into an IoE web. However, it is hard to monitor edge systems due to limited system information and limited sensors. To infer system information and provide robust monitoring capability, machine learning models were used to approximate mapping rules between different measurements. However, mapping rule learning using traditional machine learning tools is one way only, e.g., from measurement variables to the state vector variables. And, it is hard to be reverted, leading to over-fitting because of inconsistency between the forward and inverse learnings. Hence, we propose a structural deep neural network framework to provide a coherent two-way functional approximation. For physical regularization, we embed network size into the number of variables in the latent layers. We also utilize state sensors in the 'latent layer' to guide other latent variables to create state sets. The performance of reconstruction for the two-way mapping rule is validated extensively using test cases in the engineering, physics, and mathematical analysis domain.

Keywords: Edge Systems; Unobservability; Monitoring; Network Information; Auto-Physics-Encoder; Optimization; Symbolic Regression; Two-way Flow.

1. Introduction

Internet of Everything (IoE) integrates cyber-infrastructure with system physics to improve the computational and communication capabilities of the system. These are primarily used to accomplish system planning, monitoring, and control operations Ding et al. (2021). System physics is the underlying physical model of the system that governs the relationship between the measurement variables and state vectors. Due to the close interaction between cyber-infrastructure and the physics of the system, without enough sensors for monitoring, it results in process interruption and system failure. For example, active devices complement the Cyber-Physical Systems (CPS) Martínez-Castro and Jang (2018), such as the home devices and system controllers at the system edge without complete observability. Such edge system happens at the boundary areas of power grid networks Baran (2001), heat exchange networks Sheng et al. (2022), water distribution networks Tshehla et al. (2017), natural gas networks Jalving and Zavala (2018), etc. Hence, in the absence of knowledge about the control rules by the system operator on the edge, new dynamics are introduced

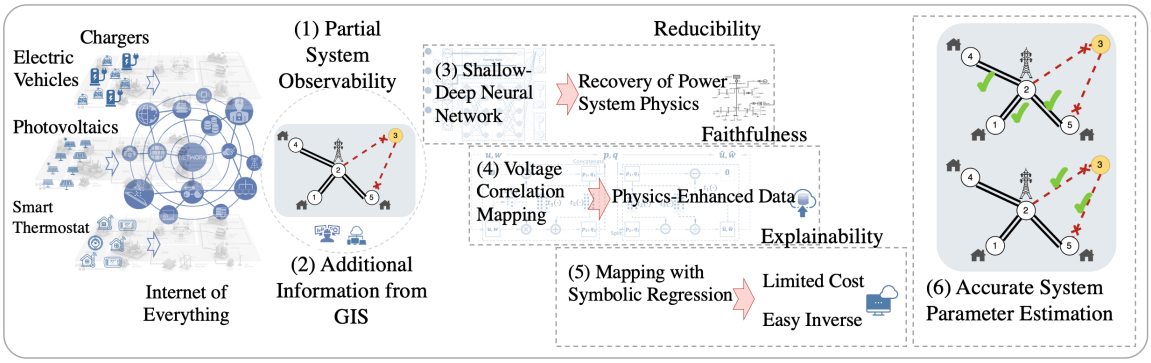

Figure 1. Framework of the constrained neural network model.

into the system. It makes robust system analysis difficult to perform. Hence, monitoring and control at the system edge is an essential component in the IoE management systems. So this paper focuses on the state estimation problem in monitoring.

Traditionally, in systems with good sensing capability, state estimation is quite useful to monitor system states Lefebvre et al. (2014). However, the prerequisite for state estimation is the need for complete system information, which does not hold especially at system edges. In that case, state estimation is performed using discriminative learning to learn the regression rule from one set of variables to another. However, there are two problems. One is the lack of physical knowledge to regularize the mapping rules for future operating points, which will create dramatically different data. The second problem is that only physical laws can create a two-way mapping with consistent results. But the learning algorithms can not handle inconsistency in the two-way mapping rule learning for physical systems. This is due to the challenge with data-driven learning algorithms in which typically the mapping is one way only, from measurement variables to the state vector variables, and can not be reverted. To resolve this issue, we design a structural deep neural network framework.

Although the system is only partially observable, we embed knowledge of the network size into the latent layer. This is a critical design in our physics-auto-encoder as our primary rule is not to compress information in the latent layer but to maintain just the right information in the latent layer, consisting of system states and latent units. Another benefit of embedding system size into the latent layer is to obtain the latent layer with a physical meaning of the system state. So, these state measurements will guide the latent units to extract a state set that can uniquely recreate all the measurements in the physical systems uniquely. To understand the framework and the outcome of the proposed data-driven model, the framework for the model-X is shown in Figure 1.

The principal contributions of the proposed method are four-fold. [i.] A two-way mapping function is used in a structural deep learning framework to introduce physical knowledge to regularize the learning of forward and inverse mapping consistency against over-fitting and unobservability. [ii.] The latent unit is created to embed knowledge of the network size into the latent layer. [iii] Improve the computational complexity by utilizing the spatial data of location and topology of nodes, which is common in physical systems. [iv.] Bound the uncertainty. Numerical results support our claim and contributions precisely. Our work opens the door for the economic monitoring of vast edge systems.

1.1. Related Work

1.1.1. Data-driven Methods to Learn System physics:

Data-driven methods enabled a major breakthrough in the state estimation algorithm Dehghanpour et al. (2018). To utilize the data-driven methods to learn system models directly from measurement data, a number of works have explored using measurement data itself. These methods use machine learning as a tool. For example, probabilistic and data-driven methods are utilized for identification of physical topology Muller et al. (2005); Singh et al. (2005, 2010); Luan et al. (2015); Hayes et al. (2016); Cavraro and Arghandeh (2018); Cavraro et al. (2019). In addition, one can embed physics in the mapping rule learning with machine learning Zhang et al. (2020); Powell et al. (2020); Guddanti et al. (2022); Yuan and Weng (2022); Li et al. (2021). Although these methods show some physical understanding of learning, they can not handle inconsistency in the two-way mapping rule learning for physical systems. Additionally, the highly important concept of state estimation is not analyzed extensively, making the learning algorithms less robust and less explainable.

1.1.2. State Estimation with Auto-Encoder with Full Observability:

When the system is observable in a well-monitored area, there are past works utilizing auto-encoder. For example, Miranda et al. (2012); Barbeiro et al. (2014) assumes full system knowledge and uses an auto-encoder to reconstruct missing data in state estimation with auto-encoders for smart grid. Different from the smart grid, Cheng et al. (2020) develops an adversarial auto-encoder for parameterized nonlinear fluid flow modeling, but it still assumes good system knowledge. Therefore, it remains open on how to design auto-encoder for systems with unobservability, with confidence.

1.1.3. Reducing Computational Complexity for Learning in Physical Systems:

Many physics-informed learning methods are time-consuming due to excessive parameter tuning process and a lot of data for training. To resolve this issue, some works have approached the problem in terms of the machine learning model selection. For example, Coelho et al. (2020) proposes a composite regularization-based network selection approach to reduce time for parameter tuning. For applications using psychological data, Epskamp and Fried (2018) uses a regularization-based model selection approach to reduce the computational complexity. In load monitoring application, Sundaray (2019) proposes a machine learning approach, based on identification of the most representative features to reduce computational complexity. But, these methods still do not take into account the system physics consideration, which can help with narrowing down the learning space further.

1.1.4. Other Works:

In dynamic systems, multiple linear models are learned in Chen and Poor (2022) on a two-stage algorithm. But, it's objective is not to learn any mappings, rather it learns the linear models that constitute sample trajectories. In physical-informed machine learning domain, the design in Lu et al. (2021) improves generalization by discovering a new operator. However, the mapping is one-way only so it lacks consistency. In symbolic regression

domain, symbolic regression is used in Cranmer et al. (2020) to generate an overall algebraic equation. But, first, it utilizes genetic algorithm, thus the method is intractable. Second, no consideration is given to prior system knowledge in library function terms. Lastly, the mapping in the work Cranmer et al. (2020) is one-way only, therefore it lacks consistency.

2. Preliminaries

In a CPS, when a node is partially observable, the state vectors are unknown. This partial observability in the topology impacts the calculation of measurement variables at the neighboring nodes. Although the measurement variables and state vectors are coupled algebraically, it becomes difficult to use a method based on a system equation solver to realize the algebraic relationship in the presence of partial observability. Therefore, in the absence of any algebraic relationship, a data-driven method needs to be employed to obtain the relationship between the measurement variables and state vectors. This mapping is utilized to determine the measurement variables associated with the unobservable nodes, which otherwise was not possible to obtain using system equations. In our proposed model-X, the measurement variables and state vectors may not necessarily be from the same observable node. The way we deal with it has been discussed in the Subsection 3.2.

State estimation relies on a general model Muscas et al. (2014), which can be represented as: $y = f(x) + \epsilon$, where y represents the vector of network measurements and pseudo-measurements, x represents the state vector, f represents the vector of non-linear measurement functions, and ϵ represents the measurement noise vector. ϵ, is usually assumed to be independent zero-mean Gaussian variable with the standard deviation of measurement values. Most state estimation programs are formulated as over-determined systems of non-linear equations, that are solved as weighted least squares (WLS) problems Maddala (1992), Lin and Davenport Jr (1997), Simpson and Monlgomery (1998), Monticelli (2000). In WLS approach, the state x is usually estimated by minimizing the weighted sum of squares of the residuals, $\arg\min_x \sum_{i=1}^{k} w_i(y_i - f_i(x))^2$, where w_i denotes weight associated with the i^{th} measurement, and k is the total number of measurements. Although, state estimation is widely adapted in power systems, the problem of limited measurements is common to CPS. So, model-X contributions can improve monitoring capability for oceanic circulation systems, climate models, aerial-vehicle monitoring, and spacecraft control systems etc.

Notation

The bold letters are used to denote vectors and vector functions; lower case letters denote scalars and scalar functions. Subscripts are used to indicate a subset. The term $\hat{x}$ indicates the expected value of x. The use of curly braces represents a set of variables. Furthermore, $\boldsymbol{y} = \{y_1, \cdots, y_n\}^T$ represents the measurement variables, and $\boldsymbol{x} = \{x_1, \cdots, x_n\}^T$ represents the state vectors, with n being the number of nodes in the CPS. In addition, $\mathcal{O}$ and $\bar{\mathbb{O}}$ represent the notations for the observable and unobservable subsystems, respectively. In the observable subsystem the corresponding set of variables are represented as $\left\{(x^i_{\mathcal{O}}, y^i_{\mathcal{O}})\right\}_{i=1}^{k}$, with k being the number of samples in the observable subsystem. Similarly, in the unobservable subsystem, the estimates of the corresponding set of variables are represented as $\left\{(x^i_{\bar{\mathbb{O}}}, y^i_{\bar{\mathbb{O}}})\right\}_{i=1}^{k'}$, with k' being the number of samples in the unobservable subsystem.

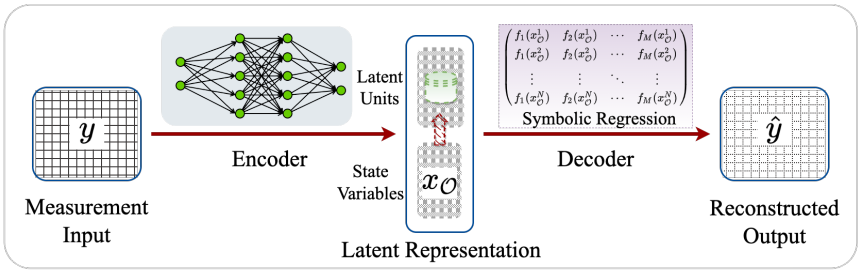

Figure 2. General architecture of the auto-encoder for model-X.

3. Proposed Method - Model-X for System Monitoring in Partial Observability

To solve forward and inverse mapping consistency, the first innovation we provide is a two-way mapping function using a structural deep learning framework. First, the mapping from measurement variables $\boldsymbol{y}$ to state vectors $\boldsymbol{x}$ is referred to as a forward mapping. Second, the mapping from state vectors $\boldsymbol{x}$ to measurement variables $\boldsymbol{y}$ is referred to as inverse mapping. Using this, the measurement variables of the system are reproducible. However, to deal with the uncertainty arising out of the unobservability in the system, intermediate mapping is used. The mapping from state vectors $\boldsymbol{x}$ to latent units is referred to as an intermediate mapping. Hence, the sensor information is used to map from the state vectors $\boldsymbol{x}_{\mathcal{O}}$ to learn the latent units $\boldsymbol{x}_{\bar{\mathbb{O}}}$, which are unobservable. This involves embedding the network size into the latent layers, which is discussed in detail in the Subsection 3.2. The numerical result for the reduction in the computational burden due to sensor information is presented in the Subsection 5.2. The latent layer consists of two components: state vectors $\boldsymbol{x}_{\mathcal{O}}$, and latent units $\boldsymbol{x}_{\bar{\mathbb{O}}}$, which are the estimates of unobservable components of the state vectors, which is discussed in detail in the Subsection 3.2.

However, neither the forward nor the intermediate mapping, estimate the system parameters explicitly. So, the next innovation we provide is performing the inverse mapping using symbolic regression to estimate the system parameters. Hence, inverse mapping from the latent variables set $\boldsymbol{x}_{\mathcal{O}}, \boldsymbol{x}_{\bar{\mathbb{O}}}$ to the measurement variables $\boldsymbol{y}$, yields the estimation for system parameters by using symbolic regression. As $\boldsymbol{x}_{\bar{\mathbb{O}}}$ is unobservable throughout the mapping, the estimate of $\boldsymbol{x}_{\bar{\mathbb{O}}}$ obtained from the intermediate mapping is considered for the inverse mapping, for estimation of system parameters. Therefore, the measurements are reconstructed by using the state vectors and the latent units in the latent layer. As the proposed data mining technique does not require any system parameters, the need for an accurate system model is eliminated as a result. The Figure 2 shows the general idea of the latent representation for model-X in the framework of auto-encoder architecture, with a focus on the two-way mapping directions. The Figure 2 shows the two-way mapping with a similar setup to the regular auto-encoder. However, the key differences between the proposed physics-auto-encoder and the regular auto-encoder model are, first, the state is partially observable in the proposed method, second the proposed model has a clear physical meaning of the latent variables, and last, part of the latent layer in the proposed approach, is observable in the domain of the cyber-physical system.

3.1. Forward Mapping: Preparing for Two-Way Information Flow

From the review, we know the system equation as $\boldsymbol{x} = f_{\boldsymbol{\theta}}(\boldsymbol{y}) + \epsilon$, for the mapping from measurement variables $\boldsymbol{y}$ to the state vectors $\boldsymbol{x}$, where the function $f_{\boldsymbol{\theta}}$ represents the underlying physics of the system, and ϵ represents the additive noise. We define forward mapping as a projection from measurement variables to the state vectors via a structural deep neural network. Therefore, the encoder is mapping the measurement variables to the state vectors in the latent layer. Mathematically, the set of $\{\boldsymbol{y}_{\mathcal{O}}, \boldsymbol{x}_{\mathcal{O}}\}$ variables are coupled algebraically. Considering this coupling, the forward mapping between these variables can be inferred upon exploring the observable subsystem. The forward mapping from measurement variables to the state vectors involves the optimization, as shown in Equation 1.

$$\arg\min_{\boldsymbol{\theta}_1} \quad \{\|f_{\boldsymbol{\theta}_1}(\boldsymbol{y}_{\mathcal{O}}) - \boldsymbol{x}_{\mathcal{O}}\|_2^2\}, \tag{1}$$

where $\boldsymbol{\theta}_1$ denotes the set of learned parameters of $f_{\boldsymbol{\theta}_1}$. The target function denoted by $f^*_{\boldsymbol{\theta}_1} : \boldsymbol{y}_{\mathcal{O}} \rightarrow \boldsymbol{x}_{\mathcal{O}}$ satisfies $\boldsymbol{x}_{\mathcal{O}} = f^*_{\boldsymbol{\theta}_1}(\boldsymbol{y}_{\mathcal{O}})$ and learns the forward mapping function.

3.2. Intermediate Mappings: Preserving Complete Information on Physical States

The forward mapping can be inferred from the coupling between observable measurements in terms of algebraic relationships. However, in the presence of partial observability, one needs additional information to infer knowledge about the partial state of the system. Therefore, in model-X, knowledge about the latent layer is vital to understanding the physics of the CPS system. Different from the normal auto-encoder, we constrain the latent layer and create an intermediate mapping in the model-X. The intermediate mapping will map from limited but observable state vectors in the latent layer to the latent units in the latent layer. And, we constrain the total number of system states, including both the state vectors and latent units, to be equal to the physical network size. This means that we can determine the number of latent units needed to make the model more physical. The mathematical formulation is as shown in Equation 2.

$$\arg\min_{\boldsymbol{\theta}_2} \|\boldsymbol{x}_{\bar{\mathbb{O}}} - f_{\boldsymbol{\theta}_2}(\boldsymbol{x}_{\mathcal{O}})\|_2^2, \tag{2}$$

where $\boldsymbol{\theta}_2$ denotes the set of learned parameters of $f_{\boldsymbol{\theta}_2}$. The target function denoted by $f^*_{\boldsymbol{\theta}_2} : \boldsymbol{x}_{\mathcal{O}} \rightarrow \boldsymbol{x}_{\bar{\mathbb{O}}}$ satisfies $\boldsymbol{x}_{\bar{\mathbb{O}}} = f^*_{\boldsymbol{\theta}_2}(\boldsymbol{x}_{\mathcal{O}})$ and learns the intermediate mapping function for obtaining state vector correlation.

3.3. Inverse Mappings: Embedding All Physical Possibilities

By using forward and intermediate mapping, the mapping function and the latent units are obtained. However, to estimate the system parameters, inverse mapping of the state vectors to the measurement variables is required. Hence, the inverse mapping objective function involves the optimization as shown in Equation 3.

$$\arg\min_{\boldsymbol{\theta}_3} \|\boldsymbol{y}_{\mathcal{O}} - f_{\boldsymbol{\theta_3}}(\boldsymbol{x}_{\mathcal{O}}, \boldsymbol{x}_{\bar{\mathbb{O}}})\|_2^2, \tag{3}$$

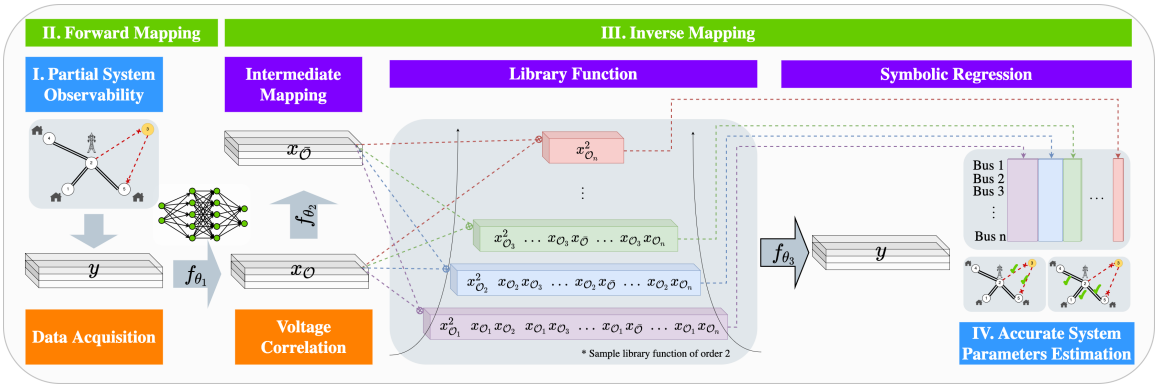

Figure 3. Architecture of the proposed model -X, a physics constrained neural network integrated with a symbolic regression.

where $\boldsymbol{\theta}_3$ denotes the set of learned parameters of $f_{\boldsymbol{\theta}_3}$. The target function denoted by $f^*_{\boldsymbol{\theta}_3}: \{\boldsymbol{x}_{\mathcal{O}}, \boldsymbol{x}_{\bar{\mathbb{O}}}\} \rightarrow \boldsymbol{y}_{\mathcal{O}}$ satisfies $\boldsymbol{y}_{\mathcal{O}} = f^*_{\boldsymbol{\theta_3}}(\boldsymbol{x}_{\mathcal{O}}, \boldsymbol{x}_{\bar{\mathbb{O}}})$ and learns the inverse mapping function. The term $\boldsymbol{x}_{\bar{\mathbb{O}}}$ indicates the estimated value of the latent unit. To understand the mappings and the logical flow of the proposed data-driven model, the basic architecture for the model-X is shown in Figure 3. The symbolic regression is performed by employing symbolic library function, Θ. The symbolic library function, Θ, consists of all possible polynomial terms resulting from the combination of state vectors $\boldsymbol{x}_{\mathcal{O}}$, and latent units $\boldsymbol{x}_{\bar{\mathbb{O}}}$, which are the estimates of unobservable components of the state vectors. The possible polynomial terms are based on the prior knowledge about the system. This includes the physical laws governing the system. This selection of underlying physics is performed by an ℓ_1 regularized regression as shown in Equation 4.

$$\arg\min_{\boldsymbol{w}} \|\boldsymbol{y}_{\mathcal{O}} - \boldsymbol{w}^T\Theta\|_2^2 + \beta\|\boldsymbol{w}\|_1, \tag{4}$$

where β is the hyper-parameter for ℓ_1 regularization with $\boldsymbol{w}$ representing weights of the variables corresponding to the symbolic function terms.

We are using inductive bias for the proposed method by generating symbolic library function terms. This considers the prior knowledge about the system as a hypothesis. However, the system interactions cannot be learned directly by using sparsity inductive bias, as the system is partially observable. Thus, in order to determine the interaction pattern for the system variables, an $\ell - 1$ regularization for sparsity of the interaction terms is used. In the Figure 3 of model-X, the functional mapping $f_{\boldsymbol{\theta}_3}$ is obtained by optimizing the inverse mapping in Equation 3 using symbolic regression. This contributes to the estimation of the physical laws corresponding to non-zero coefficient values only. The reason for using ℓ_1 regularization for inverse mapping in this work as opposed to ℓ_2 regularization is that the ℓ_1 norm performs better than a ℓ_2 norm in terms of useful feature selection.

3.4. Combined Objective for the Proposed Model X

The detailed architecture of the proposed model is visualized in Figure 3, which shows the mathematical process of learning the mappings. The proposed objective of model-X by

using a symbolic regression for inverse mapping, is described in Equation 5. This equation is obtained by combining Equations 1, 3, and 4, and represents the objective function to be optimized for estimating the system parameters.

$$\arg\min_{\psi} \|\boldsymbol{x}_{\mathcal{O}} - f_{\boldsymbol{\theta}_1}(\boldsymbol{y}_{\mathcal{O}})\|_2^2 + \|\boldsymbol{x}_{\bar{\mathbb{O}}} - f_{\boldsymbol{\theta}_2}(\boldsymbol{x}_{\mathcal{O}})\|_2^2 + \|\boldsymbol{y}_{\mathcal{O}} - \boldsymbol{w}^T\Theta\|_2^2 + \beta\|\boldsymbol{w}\|_1, \tag{5}$$

where $\psi = \{\boldsymbol{\theta}_1 \cup \boldsymbol{\theta}_2 \cup \boldsymbol{w}\}$ denotes the set of learned parameters of the model, Θ denotes the symbolic library terms obtained from the set of $\{\boldsymbol{x}_{\mathcal{O}}, \boldsymbol{x}_{\bar{\mathbb{O}}}\}$. In Equation 5, the first term performs the forward mapping operation, and the second term performs the intermediate mapping operation for estimating $\boldsymbol{x}_{\bar{\mathbb{O}}}$. The third term in Equation 5 performs the estimation of system parameters.

With this approach, system parameters are estimated from measurement variables alone. This is a fundamental change to the problem of system model approximation. In Equation 5, $\boldsymbol{x}_{\mathcal{O}}$, and $\boldsymbol{y}_{\mathcal{O}}$ are the known terms, while Θ depends on the estimates $\boldsymbol{x}_{\bar{\mathbb{O}}}$. The mapping functions $f_{\boldsymbol{\theta}_1}$, $f_{\boldsymbol{\theta}_2}$, and the model parameter $\boldsymbol{w}$ are the target variables of the optimization function. The objective of the optimization function is to obtain the term $\boldsymbol{w}$, which contains the system parameters. Thus, by combining a symbolically informed latent layer with the proposed constrained neural network, an improvement in the model approximation is achieved, which is presented in the Subsection 5.1. This improvement applies to components corresponding to both the observable and unobservable subsystems.

The algorithm for the proposed method is summarized in Algorithm 1.

Algorithm 1: Training Algorithm for Physics Constrained Symbolic Network via ℓ_1 - Norm

Data: $G = \{\boldsymbol{y}_{\mathcal{O}}, \boldsymbol{x}_{\mathcal{O}}\}$ such that G is the set of measurement variables and state vectors of the observable subsystem.

Result: Forward and inverse mapping function learning, yielding system parameters.

begin

Check: $G \neq \emptyset$

while *Error converges* **do**

1. Map $\boldsymbol{y}_{\mathcal{O}}$ to $\boldsymbol{x}_{\mathcal{O}}$ using a deep neural network.

2.*a*. Estimate $\boldsymbol{x}_{\bar{\mathbb{O}}}$ from $\boldsymbol{x}_{\mathcal{O}}$ using physically informed latent constraint: $\arg\min_{\boldsymbol{\theta_2}} \|\boldsymbol{x}_{\bar{\mathbb{O}}} - f_{\boldsymbol{\theta}_2}(\boldsymbol{x}_{\mathcal{O}})\|_2^2$;

2.*b*. Create symbolic library function using $\boldsymbol{x}_{\mathcal{O}}$ and $\boldsymbol{x}_{\bar{\mathbb{O}}}$: (Θ).

3. Combine the physically informed latent constraint with a symbolic regression: $\arg\min_{\boldsymbol{w}}\{\|\boldsymbol{y}_{\mathcal{O}} - \boldsymbol{w}^T\Theta\|_2^2 + \beta\ \|\boldsymbol{w}\|_1\}$.

4. Using sensor information, obtain the observable system parameters $w_{\mathcal{O}}$: $\arg\min_{w_{\mathcal{O}}}\{\|\boldsymbol{y}_{\mathcal{O}} - w_{\mathcal{O}}^T\boldsymbol{x}_{\mathcal{O}}\|_2^2\}$.

5. Perform multi-objective optimization upon combining the objectives from Step$-$1, and Step$-$3, and by considering the constraints from Step$-$4, to estimate the complete system parameters $(\boldsymbol{w})$.

end

end

4. Performance Guarantees for Quantifying Uncertainties

We need to measure the uncertainty of model-X for performance confidence. As latent space is typically used to generate new samples with similar properties, the latent unit obtained by intermediate mapping is used to incorporate the uncertainty, using a Bayesian perspective Kabir et al. (2018). Uncertainty quantification is presented in Theorem 1 using a Bayesian framework inspired by Kingma and Welling (2014) and Gundersen et al. (2021).

Theorem 1 (Confidence Interval for the Model-X) *For $d \in \mathbb{N}$ representing the dimensionality of $\boldsymbol{y}_{\mathcal{O}}$, Σ^{+} representing the pseudoinverse of $\mathbb{E}[\Sigma]$, and $\nu = min\ \{N_{MC},\ d\}$ degrees of freedom for the chi-squared distribution of the probability $\mathbb{P}$ for the $\chi^2(P)$ function, the confidence interval for the reconstructed $\boldsymbol{y}_{\mathcal{O}}^{(m)}\ \forall\ m \in [1, d]$ is:*

$$\left[\mathbb{E}[\boldsymbol{y}_{\mathcal{O}}^{(m)}] - \sqrt{\chi^2_{\nu}(P)}\ \|u_n^T S^{\frac{1}{2}}\|_2, \mathbb{E}[\boldsymbol{y}_{\mathcal{O}}^{(m)}] + \sqrt{\chi^2_{\nu}(P)}\ \|u_n^T S^{\frac{1}{2}}\|_2\right]$$

where u_m^T denotes the m^{th} row of the matrix U, where $\mathbb{E}[\Sigma] = USU^T$, by using singular value decomposition.

Proof The posterior distribution for the decoder part of Model-X, $\mathbb{P}\left(\boldsymbol{y}_{\mathcal{O}} \mid \boldsymbol{x}_{\mathcal{O}}\right)$ is predicted using the following.

$$\begin{aligned}\mathbb{P}\left(\boldsymbol{y}_{\mathcal{O}} \mid \boldsymbol{x}_{\mathcal{O}}\right) &= \lim_{N_{MC}\to\infty} \int \mathbb{P}\left(\boldsymbol{y}_{\mathcal{O}} \;\middle|\; \boldsymbol{x}_{\bar{\mathbb{O}}}, \boldsymbol{x}_{\mathcal{O}}\right) \mathbb{P}\left(\boldsymbol{x}_{\bar{\mathbb{O}}} \;\middle|\; \boldsymbol{x}_{\mathcal{O}}\right) d\boldsymbol{x}_{\bar{\mathbb{O}}} \\ &= \frac{1}{N_{MC}} \sum_{j=1}^{N_{MC}} \mathbb{P}\left(\boldsymbol{y}_{\mathcal{O}} \;\middle|\; \boldsymbol{x}_{\bar{\mathbb{O}}}^{(j)}, \boldsymbol{x}_{\mathcal{O}}\right).\end{aligned} \tag{6}$$

The sampling from latent space has been used to estimate the confidence region for prediction uncertainty of the trained model. Using the Monte-Carlo estimator, the mean prediction value $\mathbb{E}[\boldsymbol{y}_{\mathcal{O}}]$ and the empirical co-variance matrix $\mathbb{E}[\Sigma]$ can be obtained. The empirical standard deviation is $\hat{\sigma} = \sqrt{\text{diag}(\mathbb{E}[\Sigma])}$. To estimate the confidence interval, let us assume $\mathbb{P}\left(\boldsymbol{y}_{\mathcal{O}} \mid \boldsymbol{x}_{\mathcal{O}}\right) \sim \mathcal{N}(\mu, \sigma)$, where $\mathbb{E}[\boldsymbol{y}_{\mathcal{O}}]$ and $\mathbb{E}[\Sigma]$ are approximations to μ and σ, as obtained above from N_{MC} samples. Hence, the confidence interval estimate for $\boldsymbol{y}_{\mathcal{O}}$ is given as follows:

$$\boldsymbol{y}_{\mathcal{O}}^{(i)} \in \mathbb{R}^d : (\boldsymbol{y}_{\mathcal{O}}{}^{(j)} - \mathbb{E}[\boldsymbol{y}_{\mathcal{O}}{}^{(j)}])\ \Sigma^{+}\ (\boldsymbol{y}_{\mathcal{O}}{}^{(j)} - \mathbb{E}[\boldsymbol{y}_{\mathcal{O}}{}^{(j)}])^T \leq \chi^2_{\nu}(P), \tag{7}$$

where $\chi^2(P)$ is the quantile function for probability $\mathbb{P}$ of the chi-squared distribution with $\nu = \min\ \{N_{MC},\ d\}$ degrees of freedom. Here, $d \in \mathbb{N}$ represents the dimensionality of $\boldsymbol{y}_{\mathcal{O}}$, and Σ^{+} represents the pseudoinverse of $\mathbb{E}[\Sigma]$. Now, using singular value decomposition, $\mathbb{E}[\Sigma] = USU^T$, where u_m^T denotes the m^{th} row of the matrix U. Hence, the interval for $\boldsymbol{y}_{\mathcal{O}}^{(m)}\ \forall\ m \in [1, d]$ is:

$$\left[\mathbb{E}[\boldsymbol{y}_{\mathcal{O}}^{(m)}] - \sqrt{\chi^2_{\nu}(P)}\ \|u_n^T S^{\frac{1}{2}}\|_2, \mathbb{E}[\boldsymbol{y}_{\mathcal{O}}^{(m)}] + \sqrt{\chi^2_{\nu}(P)}\ \|u_n^T S^{\frac{1}{2}}\|_2\right]$$

■

Theorem 1 provides the upper and lower bound on the estimation error for the reconstruction of the measurement values. The bounds are defined by the expected value of the reconstructed measurements, with the deviation characterized by the quantile function for probability of the chi-squared distribution and the empirical covariance matrix of the reconstructed power values. The reconstruction is performed by considering the unobservability as latent units, which can be obtained by using the Monte-Carlo estimator. The numerical result for the uncertainty bound of the proposed method is presented in the Subsection 5.3.

5. Experiments

The contributions of this work are validated numerically for a diverse selection of test cases from the engineering, physics, and mathematical analysis domain. These include power grid transmission and distribution test cases based on MATPOWER Zimmerman et al. (2011), energy systems based on different renewable penetrations Tan and Zhang (2017), heat exchange network based on synthetic sparse parameters Davis and Hu (2011), and UF sparse matrix systems Davis and Hu (2011) based complex networks. For these test cases, the proposed method is trained by optimizing the objective function in Equation 5. To validate the performance of learning physical system representation, the proposed method is compared with Sparse Identification of Nonlinear Dynamics (SINDy) from Brunton et al. (2016) based on compressive sensing based technique as discussed in Wang et al. (2011), and with the Physics-Informed Neural Network (PINN) model from Raissi et al. (2019). For ablation study, SINDy method is used as it considers only the inverse mapping component in the analysis. The reproducibility table is provided in Supplementary Table 1.

- **Power systems test cases based on MATPOWER:** We implement the IEEE standard power system models in the high-level simulation toolbox MATPOWER Zimmerman et al. (2011) based on MATLAB. For the experiments, we considered IEEE 4-bus, 5-bus, 9-bus, 14-bus, 18-bus, 22-bus, 33-bus, 69-bus, 85-bus, and 141-bus test case systems. The test cases consist of the magnitude and phase angle values for voltage measurements along with the active and reactive power demands for the observable system nodes at multiple time instants. To use the symbolic regression-based inverse mapping, rectangular coordinates of the voltage phasors have been used to represent the power-flow mappings based on Sundaray and Weng (2022).

- **Heat exchange network based on a 207-node system using synthetic sparse parameters:** We implement a heat exchange network based on Davis and Hu (2011). The test case consists of the total heat supplied to the system, and the change in temperature of the system for the observable system nodes at multiple time instants. The total heat supplied to the system is considered as the measurement, and change in temperature of the system is considered as the state vector. We denote it by HE 207. The heat exchange equation is the system physics for generating simulated data.

- **UF sparse matrix-based system:** The UF sparse matrix-based complex network system Davis and Hu (2011) is used to validate model-X. We considered 15-node, 98-node, and 274 node test case systems, and denote those by UFS 15, UFS 98, and UFS 274 respectively. The state vector and measurement values are simulated based

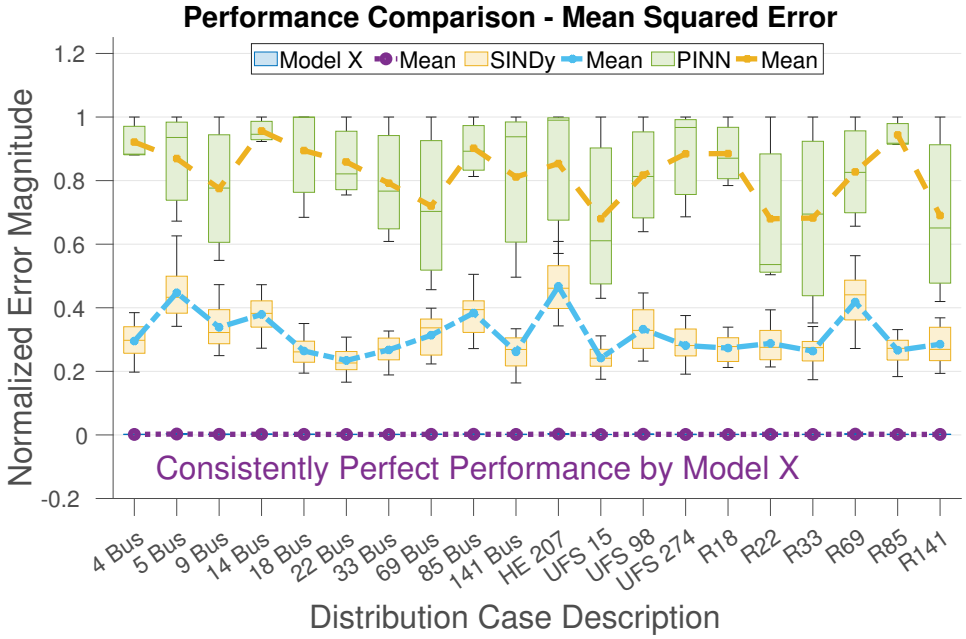

Figure 4. Comparison of system parameter estimation in a partially observable system.

on the system physics and the sparse coefficient matrix. The test cases consist of the explanatory variable and response variable for the observable system nodes at multiple time instants. The response variable of the system is considered the measurement, and the explanatory variable of the system is considered the state vector.

- **Renewable penetration-based energy systems test cases:** To validate robustness of model-X, we implement power system models integrated with renewable penetration Tan and Zhang (2017). We considered 18-bus, 22-bus, 33-bus, 69-bus, 85-bus, and 141-bus test case systems for renewable penetration. The test cases are denoted by RXX, where XX denotes the number of buses. The test cases consist of the magnitude and phase angle values for voltage measurements along with the active and reactive power demands for the observable system nodes at multiple time instants.

5.1. Robust Reconstruction: Using Two-way Information Flow

By using model-X, the estimation of parameters corresponding to the nodes which are not interacting with the unobservable bus directly is estimated accurately. In addition, the parameters associated with the unobservable nodes are also estimated, which was otherwise impossible to find using simple regression. The analysis is performed on multiple CPS systems, and the mean and variance of the error values are plotted in Figures 4. The performance comparison of model-X against comparative methods is shown to validate the consistently perfect system parameter estimation capability of model-X, which proves the forward and inverse mapping capability of model-X.

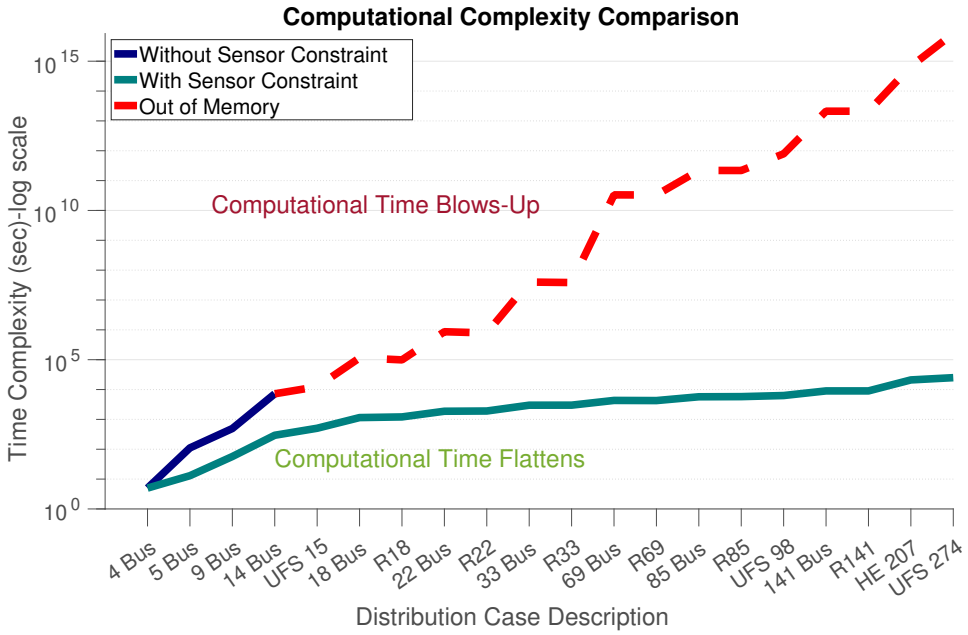

Figure 5. Comparison of model-X computational time.

5.2. Improvement in Computational Complexity: Embedding Constrained network size into Latent Layer using Sensor Information

By using sensor data as a constraint in Equation 5, the number of system states is determined for estimating the unobservability. Obtaining an adequate number of system states results in reducing the number of library functions. This helps in reducing the complexity of optimization using symbolic regression. It results in improvement of the number of parameters with increase in dimension, from exponential growth to linear growth. The comparison of computational time with and without using sensor information is shown in Figure 5. This validates the significant improvement in computational complexity of model-X. In Figure 5, the OoM (Out-of-Memory) points are obtained by using non-linear regression.

5.3. Performance Guarantee for Quantifying Uncertainty of Model-X: Using Latent Layers Constrained Mapping Design

The estimation of parameters corresponding to the nodes which are directly interacting with the unobservable node is obtained accurately by using the two-way information flow, which otherwise would not be possible using prevalent methods. The confidence interval (CI) for the performance of model-X in terms of the two-way information flow is shown in Figure 6. It is important to note here that, the y-axis scale while obtaining the confidence interval is determined by data points in terms of estimation error for the posterior distribution. So, the plot captures the mean value of the posterior estimation error. However, as certain points in terms of the posterior estimation error also fall beyond the mean value due to the variable standard deviation, this is captured by the confidence interval region as shown in the Figure 6.

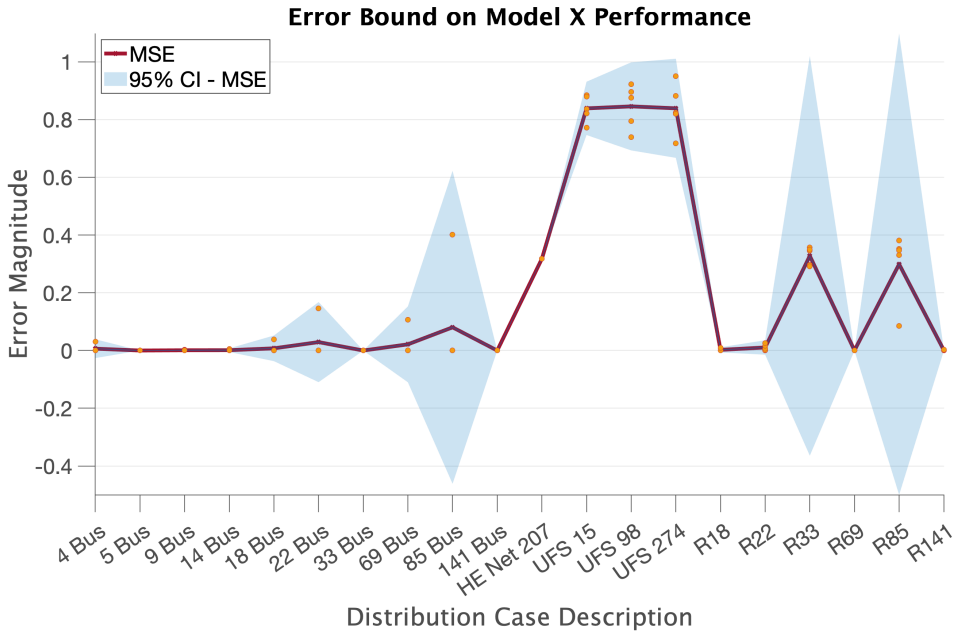

Figure 6. Confidence of system parameter estimation in partial observability.

6. Conclusion

We present a solution to the problem of providing robust monitoring capability for cyber-physical systems (CPS) in data-limited scenarios by inferring system physics information. It has played a key role in a variety of research directions. These include controllability of edge systems, state estimation and attack detection in CPS, enhancing the functionality and performance of the Internet of Everything (IoE), etc. This work shows that it is possible to achieve superior mapping capability to learn the underlying physical information of the systems, even with limited observability using consistent two-way mapping and the latent layer design with network size and latent units. The proposed method shows strong performance on the benchmark method. In addition to the improved mapping performance, the method focus on understanding the relationship of latent units to measurements. Based on the numerical results, the proposed method is capable of estimating the system parameters with high accuracy in presence of partial observability of the system. It involves all system components, including those interacting directly with the unobservability. The improvement in the computational complexity achieved by embedding the network size into the latent layers applies to a wide range of results using sensor information. It suggests that the proposed model can adapt to any dimensionality of CPS. Improvement of the mapping and computational capability ensures a robust and accurate model for a sustainable and reliable CPS operation. This model provides confidence in the mapping. Thus, the model has the potential to form the next generation of CPS management systems with design consistency, maximized physical explainability, and confidence. This will instill trust in the AI for IoE on the system edges with unobservability.

Acknowledgments

The authors acknowledge support in part by the Department of Energy (DOE) under grants DE-AR00001858-1631 and DE-EE0009355, the National Science Foundation (NSF) under grants ECCS-1810537 and ECCS-2048288, and the Air Force Office of Scientific Research under grant AFOSR FA9550-22-1-0294.

References

Mesut E. Baran. Challenges in state estimation on distribution systems. *IEEE Power Engineering Society Transmission and Distribution Conference*, Aug 2001.

P. N. Pereira Barbeiro, J. Krstulovic, H. Teixeira, J. Pereira, F. J. Soares, and J. P. Iria. State estimation in distribution smart grids using autoencoders. Mar 2014.

Steven L. Brunton, Joshua L. Proctor, and J. Nathan Kutz. Discovering governing equations from data by sparse identification of nonlinear dynamical systems. *Proceedings of the National Academy of Sciences*, Mar 2016.

Guido Cavraro and Reza Arghandeh. Power distribution network topology detection with time-series signature verification method. *IEEE Transactions on Power Systems*, Jul 2018.

Guido Cavraro, Vassilis Kekatos, and Sriharsha Veeramachaneni. Voltage analytics for power distribution network topology verification. *IEEE Transactions on Smart Grid*, Jan 2019.

Yanxi Chen and H. Vincent Poor. Learning mixtures of linear dynamical systems. volume 162 of *Proceedings of Machine Learning Research*, pages 3507–3557, July 2022.

M Cheng, F Fang, CC Pain, and IM Navon. An advanced hybrid deep adversarial autoencoder for parameterized nonlinear fluid flow modelling. *Computer Methods in Applied Mechanics and Engineering*, Aug 2020.

Frederico Coelho, Marcelo Costa, Michel Verleysen, and Antônio P. Braga. LASSO multi-objective learning algorithm for feature selection. *Soft Computing*, Feb 2020.

Miles D. Cranmer, Alvaro Sanchez-Gonzalez, Peter W. Battaglia, Rui Xu, Kyle Cranmer, David N. Spergel, and Shirley Ho. Discovering symbolic models from deep learning with inductive biases. Dec 2020.

Timothy A Davis and Yifan Hu. The university of florida sparse matrix collection. *ACM Transactions on Mathematical Software*, Nov 2011.

Kaveh Dehghanpour, Zhaoyu Wang, Jianhui Wang, Yuxuan Yuan, and Fankun Bu. A survey on state estimation techniques and challenges in smart distribution systems. *IEEE Transactions on Smart Grid*, Sep 2018.

Derui Ding, Qing-Long Han, Xiaohua Ge, and Jun Wang. Secure state estimation and control of cyber-physical systems: A survey. *IEEE Transactions on Systems, Man, and Cybernetics: Systems*, Jan 2021.

Sacha Epskamp and Eiko I. Fried. A tutorial on regularized partial correlation networks. *Psychological Methods*, Dec 2018.

Kishan Prudhvi Guddanti, Yang Weng, and Baosen Zhang. A matrix-inversion-free fixed-point method for distributed power flow analysis. *IEEE Transactions on Power Systems*, Jan 2022.

Kristian Gundersen, Anna Oleynik, Nello Blaser, and Guttorm Alendal. Semi-conditional variational auto-encoder for flow reconstruction and uncertainty quantification from limited observations. *Physics of Fluids*, Jan 2021.

Barry Hayes, Alberto Escalera, and Milan Prodanovic. Event-triggered topology identification for state estimation in active distribution networks. *IEEE PES Innovative Smart Grid Technologies Conference Europe*, Oct 2016.

Jordan Jalving and Victor M. Zavala. An optimization-based state estimation framework for large-scale natural gas networks. *Industrial & Engineering Chemistry Research*, Mar 2018.

H. M. Dipu Kabir, Abbas Khosravi, Mohammad Anwar Hosen, and Saeid Nahavandi. Neural network-based uncertainty quantification: A survey of methodologies and applications. *IEEE Access*, Jun 2018.

Diederik P. Kingma and Max Welling. Auto-encoding variational bayes. *International Conference on Learning Representations*, May 2014.

S. Lefebvre, J. Prevost, and L. Lenoir. Distribution state estimation: A necessary requirement for the smart grid. *IEEE PES General Meeting*, Jul 2014.

Haoran Li, Yang Weng, Yizheng Liao, Brian Keel, and Kenneth E. Brown. Distribution grid impedance & topology estimation with limited or no micro-PMUs. *International Journal of Electrical Power & Energy Systems*, Jul 2021.

Chowhong Lin and Ernest C Davenport Jr. A weighted least squares approach to robustify least squares estimates. *Annual Meeting of the American Educational Research Asociation*, Mar 1997.

Lu Lu, Pengzhan Jin, Guofei Pang, Zhongqiang Zhang, and George Em Karniadakis. Learning nonlinear operators via DeepONet based on the universal approximation theorem of operators. *Nature Machine Intelligence*, Mar 2021.

Wenpeng Luan, Joshua Peng, Mirjana Maras, Joyce Lo, and Brian Harapnuk. Smart meter data analytics for distribution network connectivity verification. *IEEE Transactions on Smart Grid*, Jul 2015.

Gangadharrao S Maddala. *Introduction to economics*. Macmillan, 1992.

Rosana E Martínez-Castro and Shinae Jang. Structural cyber-physical systems: A confluence of structural health monitoring and control technologies. Feb 2018.

Vladimiro Miranda, Jakov Krstulovic, Hrvoje Keko, Cristiano Moreira, and Jorge Pereira. Reconstructing missing data in state estimation with autoencoders. *IEEE Transactions on Power Systems*, May 2012.

A. Monticelli. Electric power system state estimation. *Proceedings of the IEEE*, Feb 2000.

Heloisa H. Muller, Marcos J. Rider, Carlos A. Castro, and V. Leonardo Paucar. Power flow model based on artificial neural networks. *IEEE Russia Power Tech*, Jun 2005.

Carlo Muscas, Marco Pau, Paolo Attilio Pegoraro, and Sara Sulis. Effects of measurements and pseudomeasurements correlation in distribution system state estimation. *IEEE Transactions on Instrumentation and Measurement*, Dec 2014.

Siobhan Powell, Alyona Ivanova, and David Chassin. Fast solutions in power system simulation through coupling with data-driven power flow models for voltage estimation. *arXiv*, abs/2001.01714, Jan 2020.

M. Raissi, P. Perdikaris, and G.E. Karniadakis. Physics-informed neural networks: A deep learning framework for solving forward and inverse problems involving nonlinear partial differential equations. *Journal of Computational Physics*, Feb 2019.

Tongtian Sheng, Guanxiong Yin, Bin Wang, Qinglai Guo, Jinni Dong, Hongbin Sun, and Zhaoguang Pan. State estimation approach for combined heat and electric networks. *CSEE Journal of Power and Energy Systems*, Jun 2022.

James R Simpson and Douglas C Monlgomery. A performance-based assessment of robust regression methods. *Communications in Statistics-Simulation and Computation*, Jan 1998.

D. Singh, J.P. Pandey, and D.S. Chauhan. Topology identification, bad data processing, and state estimation using fuzzy pattern matching. *IEEE Transactions on Power Systems*, Aug 2005.

Ravindra Singh, Efthymios Manitsas, Bikash C Pal, and Goran Strbac. A recursive bayesian approach for identification of network configuration changes in distribution system state estimation. *IEEE Transactions on Power Systems*, Aug 2010.

Priyabrata Sundaray. Machine learning approach to event detection for load monitoring. *Research Thesis, University of Wisconsin-Madison*, Dec 2019.

Priyabrata Sundaray and Yang Weng. Alternative auto-encoder for state estimation in distribution systems with unobservability. *IEEE Transactions on Smart Grid*, Sep 2022.

Jin Tan and Yingchen Zhang. Coordinated control strategy of a battery energy storage system to support a wind power plant providing multi-timescale frequency ancillary services. *IEEE Transactions on Sustainable Energy*, Jul 2017.

Kgaogelo S. Tshehla, Yskandar Hamam, and Adnan M. Abu-Mahfouz. State estimation in water distribution network: A review. Jul 2017.

Wen-Xu Wang, Rui Yang, Ying-Cheng Lai, Vassilios Kovanis, and Celso Grebogi. Predicting catastrophes in nonlinear dynamical systems by compressive sensing. *Physical Review Letters*, Apr 2011.

Jingyi Yuan and Yang Weng. Support matrix regression for learning power flow in distribution grid with unobservability. *IEEE Transactions on Power Systems*, Mar 2022.

Jiawei Zhang, Yi Wang, Yang Weng, and Ning Zhang. Topology identification and line parameter estimation for non-PMU distribution network: A numerical method. *IEEE Transactions on Smart Grid*, Sep 2020.

Ray Daniel Zimmerman, Carlos Edmundo Murillo-Sanchez, and Robert John Thomas. MATPOWER: Steady-state operations, planning, and analysis tools for power systems research and education. *IEEE Transactions on Power Systems*, Feb 2011.